Monthly Notices
of the
ROYAL ASTRONOMICAL SOCIETY

Mon. Not. R. Astron. Soc. **415,** 563–575 (2011) doi:10.1111/j.1365-2966.2011.18728.x

High-resolution elemental abundance analysis of the Hyades supercluster⋆

G. M. De Silva,[1]† K. C. Freeman,[2] J. Bland-Hawthorn,[3] M. Asplund,[4] M. Williams[5] and J. Holmberg[6]

[1]*Australian Astronomical Observatory, PO Box 296, NSW 1710, Australia*
[2]*Research School of Astronomy and Astrophysics, Mount Stromlo Observatory, Australian National University, ACT 2611, Australia*
[3]*Institute of Astronomy, School of Physics, University of Sydney, NSW 2006, Australia*
[4]*Max Planck Institute for Astrophysics, Karl-Schwarzschild-strasse 1, Garching 85741, Germany*
[5]*Astrophysikalisches Institut Potsdam, An der Sternwarte 16, Potsdam D-14482, Germany*
[6]*The Niels Bohr Institute, Astronomy Group, Juliane Maries Vej 30, 2100 Copenhagen, Denmark*

Accepted 2011 March 16. Received 2011 March 16; in original form 2011 January 20

ABSTRACT

The existence of a kinematically defined moving group of stars centred at $U = -40, V = -17$ km s^{-1}, referred to as the Hyades supercluster, has been suggested to be the debris of an originally large star-forming event, with its core being the present-day Hyades open cluster. Using high-resolution UV-Visual Echelle Spectrograph (UVES) spectra, we present the elemental abundances for a range of alpha, Fe-peak and neutron-capture elements for 26 proposed supercluster stars. Our results show that the sample stars display a heterogeneous abundance distribution, with a clump around [Fe/H] $= +0.15$. We also calculate stellar radial velocities and U, V, W space velocities. Enforcing strict chemical and kinematical membership criteria, we find that four supercluster stars share the Hyades open cluster abundances and kinematics, while many of the remaining stars fit the disc field kinematics and abundance range. We discuss our findings in the context of the Hyades supercluster being a dispersed star-forming remnant, a stellar stream of purely dynamical origin or a result of several processes.

Key words: Galaxy: abundances – Galaxy: disc – open clusters and associations: individual: Hyades supercluster.

1 INTRODUCTION

To obtain a detailed physical understanding of the events that shaped the Galactic disc, we must examine its individual stars. The chemical abundances as measured from stellar photospheres can be indicative of the conditions of a star's birth site. Different chemical elements are synthesized during different stages of stellar evolution and are distributed to the interstellar medium via supernova explosions or stellar winds. By studying the abundances of these elements we can estimate the frequency and importance of each synthesis process. Therefore the chemical abundance patterns within the disc stars can be regarded as a fossil imprint and hold key information of the events that took place during the disc's formation and evolutionary history. The long-term goal of Galactic Archaeology is to reconstruct the original star-forming events of the Galaxy. Employing the technique of chemical tagging (Freeman & Bland-Hawthorn 2002) to disc stars, one can identify the now-dispersed ancient stellar aggregates, the building blocks of the Galactic disc.

Candidates for such fossil stellar aggregates are moving groups and superclusters, where their stellar members are unbound but share a common motion around the Galaxy. Analogous to stellar streams in the Galaxy halo which are remnants of merged satellites, old moving groups and superclusters may represent the ancient stellar building blocks of the disc. A strong advocate for the reality of these groups was Olin Eggen, who identified several moving groups and superclusters (Eggen 1958–1998). With the availability of the *Hipparcos* catalogue of parallaxes and proper motions it became possible to study these substructures in unprecedented detail. Several studies have analysed the *Hipparcos* catalogue and re-identified the classical groups as well as found new ones (Antoja et al. 2008; Bovy, Hogg & Roweis 2009; Zhao, Zhao & Chen 2009). Essentially, all of these studies have focused purely on the dynamical/kinematical nature of the substructures in the disc.

Thus moving groups and superclusters provide disc substructures that can be identified through kinematics. However, it is not yet clear if all, or indeed the majority, of these substructures actually originate from star-forming clusters that have or are in the process of being dispersed. Such substructures can equally well be the result of the dynamical interaction between the stars in the field and the central bar or the spiral structure of the Milky Way (see e.g. Dehnen 1998).

⋆Based on observations made at the European Southern Observatory, Paranal, Chile (ESO programmes 080.D-0094(A) and 381.B-0045(A)).

†E-mail: gdesilva@aao.gov.au

Therefore not all kinematically defined disc substructures represent the debris of a single star formation event.

1.1 The Hyades supercluster

The existence of a dispersed kinematically defined group of stars associated with the Hyades open cluster was proposed by Eggen (1970), as a part of a larger star-forming event, where the outer cluster stars have dispersed into the Hyades supercluster, leaving only its core members in the present-day Hyades open cluster. The existence of the kinematically defined Hyades supercluster is well established observationally (e.g. in *Hipparcos*, RAVE and Geneva–Copenhagen survey), where a concentration of stars are found at $U \sim -40$ km s^{-1} and $V \sim -20$ km s^{-1} in the U–V velocity plane. Throughout this article we consider the direction of the U-velocity to be positive towards the Galactic centre. However, many studies suggest that this overdensity of stars consists of a mixture of field stars that have been resonantly swept up by a passing spiral wave and is not the result of a dispersed stellar aggregate (Famaey et al. 2005; Bovy & Hogg 2010; Minchev et al. 2010).

With kinematical information alone it is difficult to address the reality of dispersed stellar aggregates. The dissipative formation and dynamical evolution of the Galaxy means much of the kinematical information is limited to the last event of scattering, where the original kinematical information has been modified as a result of latter events. Therefore only the most recent events can be traced with kinematics, masking the initial identity. However, the chemical information in the form of elemental abundances of individual stars remains preserved. Present-day open clusters are chemically homogeneous (De Silva et al. 2006; Pancino et al. 2010), which demonstrates that the stars' natal chemical composition is unaltered. Therefore, along with kinematical information, chemical probing of moving groups and superclusters offers the possibility to determine their initial identity. Detailed abundance study of the HR 1614 moving group (De Silva et al. 2007a) demonstrated that its member stars are chemically homogeneous and clearly distinguishable from the disc field stars, indicating that it is a dispersed relic of an earlier star-forming event (see also Bubar & King 2010, for the case of Wolf 630 moving group). Conversely, an example of a dynamically defined group is the Hercules stream, which is not chemically homogeneous and its abundance patterns are not distinguishable from the field stars (Bensby et al. 2007). When inspected in velocity space alone, both the HR 1614 moving group and the Hercules stream satisfy the requirements for a dispersing cluster remnant, while chemical probing shows that they have very different origins. These examples demonstrate that chemical information is essential to identify dispersed group members, and that dynamical information alone cannot be used to uncover the true history behind any comoving group of stars in the disc.

Despite the wealth of information obtainable via chemical probing, elemental abundance analysis of the kinematically defined moving groups is not available in the literature, possibly due to the larger effort required to measure accurate abundances. In this paper we present the high-resolution elemental abundances for a sample of proposed Hyades supercluster stars and examine its possible origins.

2 SAMPLE SELECTION

Assuming that the Hyades supercluster is a part of a larger structure produced by a dissolving star formation site, we can expect that the site would dissolve along a dispersion orbit. These paths along which a gently disrupting system would dissolve, can be approximated by closed ellipses when viewed from a frame rotating at the local value of $\Omega - \kappa/2$, where Ω is the local angular velocity of rotation near the Sun and κ is the epicyclic frequency. The stars move clockwise around these ellipses with angular velocity approximately $\kappa/2$ and gradually spread out around them. In this work, the adopted velocity of Hyades supercluster stars near the Sun was $U = -40, V = -17$ km s^{-1}, consistent with the currently accepted motion of the Hyades open cluster and the corresponding overdensity regions seen in the Geneva–Copenhagen survey.

Wilson (1990) observed low-latitude K giant stars from the Michigan catalogue (Houk 1982) in the expected direction of the Hyades supercluster dispersion orbit. The observations were carried out using the coudé spectrograph on the Mt Stromlo Observatory 74-inch telescope. The data of $R \sim 20\,000$ centred at 5200 Å were cross-correlated against template spectra to derive metallicities and radial velocities. Wilson found a concentration of stars in the abundance range -0.2 to -0.1 lying close to the Hyades dispersion orbit loci in the radial velocity–longitude plane, which he interpreted as being stars associated with the dispersing Hyades systems. The currently accepted Hyades open cluster metallicity is [Fe/H] $= +0.13$ dex based on high-resolution abundances (Paulson Sneden & Cochran 2003; Primas et al., in preparation). While we cannot accurately compare high-resolution Fe abundances with the early metallicity derivations due to likely zero-point offsets, it is interesting that a concentration of stars was found along the dispersion orbits in this metallicity bin.

We selected stars likely to be dispersing Hyades supercluster stars based on Wilson's results for high-resolution observations. Our analysis will test the hypothesis of the disrupting system discussed above. We also targeted F-type probable member stars as published in Eggen (1998), which had *Hipparcos* identification. Table 1 lists the IDs, coordinates, V magnitude and colour for all the observed stars. In the last column of Table 1, E98 indicates stars selected from Eggen (1998) and W indicates those selected from Wilson's thesis.

3 OBSERVATIONS

High-resolution and high signal-to-noise ratio spectra of probable members of the Hyades supercluster were observed using the VLT UV-Visual Echelle Spectrograph (UVES) at UT2 in the framework of programmes 080.D-0094(A) and 381.B-0045(A). A total of 45 probable member stars were submitted for service mode observations, using the UVES Red arm standard setting at 520 nm which provides complete spectral coverage from 4200 to 6200 Å, and employed a 0.8-arcsec slit to achieve a spectral resolving power of 60 000. The typical signal-to-noise (S/N) ratio was 100 pixel^{-1}. The data were reduced with the latest UVES ESO-MIDAS pipeline. The resulting spectra were normalized using the *continuum* task in the IRAF package.[1]

Out of the total 45 targets observed, only 26 could be used for abundance analysis. The other 19 stars showed broadened spectral lines due to high rotation and were hence discarded from further analysis. 17 of these stars were from Eggen (1998), likely to be

[1] IRAF is distributed by the National Optical Astronomy Observatory, which is operated by the Association of Universities for Research in Astronomy, Inc., under cooperative agreement with the National Science Foundation.

Table 1. Total sample of observed stars.

ID	RA	Dec.	V	$B-V$	Notes
HD 25102	03 59 40.4935	+10 19 49.448	6.34	0.42	E98
HD 26737	04 14 30.4203	+22 27 06.713	7.04	0.43	E98
HD 27429	04 20 25.1095	+18 44 33.390	6.09	0.38	E98
HD 27534	04 21 32.2686	+18 25 03.297	6.78	0.45	E98
HD 27848	04 24 22.2727	+17 04 44.225	6.95	0.46	E98
HD 27991	04 25 37.3171	+15 56 27.636	6.45	9.45	E98
HD 28394	04 29 20.5531	+17 32 41.766	7.01	0.51	E98
HD 28608	04 30 57.1723	+10 45 06.365	7.02	0.47	E98
HD 28736	04 32 04.8091	+05 24 36.126	6.35	0.43	E98
HD 30912	04 52 47.1170	+27 53 50.947	5.97	0.34	E98
HD 50643	06 53 21.8408	−18 55 58.238	6.13	0.16	E98
HD 69511	08 15 58.8226	−35 54 11.486	6.16	1.57	W
HD 69836	08 17 30.5546	−35 10 14.009	8.57	1.08	W
HD 72320	08 30 29.1090	−42 54 34.058	8.95	0.94	W
HD 72630	08 32 23.7142	−41 29 53.544	9.49	1.01	W
HD 73657	08 37 48.1209	−42 19 11.404	7.85	1.18	W
HD 73829	08 38 44.3768	−43 08 16.205	9.42	1.27	W
HD 74165	08 40 53.4114	−40 40 55.841	9.12	1.16	W
HD 74166	08 40 42.6510	−42 20 26.606	7.62	1.29	W
HD 74529	08 42 43.4206	−47 14 25.097	8.41	1.19	W
HD 74900	08 45 13.1890	−41 52 44.224	7.96	1.17	W
HD 75058	08 46 21.9930	−38 18 19.552	8.94	1.08	W
HD 75171	08 44 29.9575	−65 49 31.544	6.03	0.19	E98
HD 76128	08 52 47.7716	−41 25 49.269	7.90	1.40	W
HD 77117	08 58 37.7029	−47 04 17.465	9.46	0.52	W
HD 77241	08 59 30.6086	−48 49 11.118	9.98	1.02	W
HD 78002	09 04 19.8280	−43 20 22.225	9.45	1.05	W
HD 78097	09 04 46.8967	−44 48 37.337	7.61	1.63	W
HD 78204	09 05 02.8562	−50 52 45.128	9.95	1.04	W
HD 78402	09 06 16.1539	−49 04 41.490	9.88	0.93	W
HD 78528	09 06 57.8364	−49 38 22.415	8.86	1.59	W
HD 78959	09 09 29.8423	−44 33 59.972	7.80	1.75	W
HD 80571	09 19 07.6889	−46 38 22.151	7.88	1.09	W
HD 80911	09 20 41.4133	−50 42 09.173	8.56	1.73	W
HD 81278	09 22 52.1556	−52 08 04.264	8.48	1.08	W
HD 82438	09 30 12.8630	−52 01 55.341	9.00	1.64	W
HD 83234	09 35 04.8294	−54 36 14.833	8.56	1.42	W
HD 84598	09 44 53.2380	−50 00 36.850	7.45	0.97	W
HD 86757	09 58 56.8698	−54 37 13.983	8.36	1.59	W
HD 97840	11 15 02.4004	−33 19 03.880	6.99	0.32	E98
HD 112734	12 58 33.8230	+28 19 10.449	6.94	0.26	E98
HD 117374	13 40 55.4795	−85 47 09.756	5.56	0.17	E98
HD 121164	13 53 10.2822	+28 38 53.273	5.91	0.19	E98
HD 122721	14 04 14.5737	−33 06 19.948	9.16	1.06	E98
HD 218475	23 08 22.9309	−07 16 01.221	8.31	0.33	E98

F-type dwarfs, and two stars were K giants from Wilson's thesis. Of the 26 sharp-lined spectra, only one star was from the sample of Eggen (1998).

4 ABUNDANCE ANALYSIS

4.1 Model atmospheres and spectral lines

The elemental abundances were derived based on equivalent (EW) measurements and spectral synthesis, making use of the latest version of the MOOG code (Sneden 1973). The EWs were measured by fitting a Gaussian profile to each line using the interactive SPLOT function in IRAF. On occasions the local continuum level was adjusted by eye. Abundances of Mn, Ba, La and Ce were derived using the *synth* routine of the MOOG code to account for line blending and hyperfine structures. Interpolated Kurucz model atmospheres based on the ATLAS9 code (Castelli, Gratton & Kurucz 1997) with no convective overshoot were used throughout this study.

Table 2. Line list. The full table is available with the online version of the article (see Supporting Information).

Wavelength (Å)	Species	LEP (eV)	log *gf*
4517.524	Fe I	3.071	−1.86
4547.847	Fe I	3.546	−1.01
4566.515	Fe I	3.301	−2.38
4587.127	Fe I	3.573	−1.74
–	–	–	–
–	–	–	–

The line list used in this analysis is given in Table 2 and is available in the online version of this article (see Supporting Information). The employed lines and *gf* values for Fe, Na, Mg, Al, Si, Ca, Ti, Cr, Ni and Zn were a subset of the lines used by Bensby, Feltzing & Lundström (2003), where their main source of the Fe I line data is the laboratory measurements by the Oxford group (Blackwell et al. 1979a; Blackwell, Petford & Shallis 1979b; Blackwell, Lynas-Gray & Smith 1995, and references therein). We chose this particular Fe line list as it will better enable comparison of our results with those of the disc field stars by Bensby et al. (2003, 2005), as well as with the Hyades open cluster abundances of Primas et al. (in preparation) who employ the same line list. The lines of S, Sc, Co and Zr were adopted from Gratton et al. (2001). For Mn and Ba, the line data were taken from Prochaska & McWilliam (2000) and Prochaska et al. (2000) respectively and include the effects of hyperfine splitting. The La and Ce line data were obtained via the VALD data base[2] (Piskunov et al. 1995; Ryabchikova et al. 1997; Kupka et al. 1999, 2000).

4.2 Stellar parameters and elemental abundances

We derive the stellar parameters based on spectroscopy. Abundances for all Fe I and II lines were computed from the measured EWs. Effective temperature ($T_{\rm eff}$) was derived by requiring excitation equilibrium of the Fe I lines. Microturbulence was derived from the condition that Fe I lines show no trend with EW. Surface gravity ($\log g$) was derived via ionization equilibrium, i.e. requiring the abundances from Fe I equals Fe II. The resulting stellar parameters are given in Table 3. For comparison we also calculated stellar temperatures based on photometry. Using the $B-V$ colour value and adopting [Fe/H] = 0.0, we use equation (4) of Alonso, Arribas & Martinez-Roger (1999) to derive photometric stellar temperatures. We find that the spectroscopic effective temperatures are on average hotter by approximately 150 K compared to the photometric values. Fig. 1 plots the photometric effective temperature against the spectroscopic values.

To check for possible trends with effective temperature, we plot the spectroscopic [Fe/H] versus the spectroscopic effective temperature in Fig. 2. The dotted line represents the solar metallicity (adopted from Asplund et al. 2009) and the dashed line represents the Hyades open cluster metallicity of [Fe/H] = 0.15 [note that Paulson et al. (2003) finds the Hyades open cluster to have [Fe/H] = 0.13, but taking into account the difference in the solar metallicity used in this study, we place the Hyades open cluster at

[2] http://ams.astro.univie.ac.at/vald/

Table 3. Spectroscopic stellar parameters.

Star ID	$T_{\rm eff}$ (K)	log g (cm s^{-2})	ξ (km s^{-1})
HD 86757	4100	0.5	2.3
HD 84598	5050	2.8	1.45
HD 83234	4300	2.0	1.6
HD 82438	4100	0.5	2.6
HD 81278	4900	3.0	1.1
HD 80911	4200	0.7	2.3
HD 80571	4900	2.5	1.4
HD 78959	4150	1.2	2.2
HD 78528	4050	1.2	1.7
HD 78402	4900	2.5	1.1
HD 78204	5050	2.8	1.5
HD 78097	4150	0.6	2.4
HD 78002	5000	3.0	1.4
HD 77241	4600	2.3	1.6
HD 76128	4650	2.8	1.3
HD 75058	4650	2.8	1.2
HD 74900	4650	2.6	1.5
HD 74529	4650	2.6	1.4
HD 74166	4300	1.8	1.8
HD 74165	4600	2.4	1.5
HD 73829	4650	2.5	1.45
HD 73657	4500	2.2	1.7
HD 72630	4950	3.0	1.4
HD 72320	5200	3.2	1.4
HD 69836	4750	2.5	1.45
HD 122721	4650	2.5	1.25

[Fe/H] = 0.15]. The six coolest stars show a sudden drop in metallicity. As there is no clear Fe abundance trends with $T_{\rm eff}$, it is unlikely that we are seeing a temperature-dependent effect or non-LTE effects.

The reason for the large drop in [Fe/H] for the cool stars is unclear. We recomputed the Fe abundances for these cool stars using the photometric $T_{\rm eff}$ values. We find this results in Fe I abundances increasing closer to the warmer star abundance levels; however, large deviations of the order of +0.2 dex are seen between Fe I and Fe II abundances, where Fe II is larger. Studies of cool K-dwarfs in the Hyades open clusters and in the disc field have reported similar discrepancies between Fe I and Fe II and other ionized elements when adopting photometric temperature scales (Allende Prieto et al. 2004; Yong et al. 2004). Chromospheric activities associated with magnetic fields are thought to give rise to these effects in the cool dwarfs. However, our targets are K-giants, and we are not aware of any studies indicating such discrepancies among cool giants. Given the large Fe I and Fe II discrepancies when using the photometric temperatures, and the significantly lower metallicities resulting from the spectroscopic parameters, we cannot rely on either set of parameters for the cool stars. We hope to further investigate this issue in a dedicated study. As this is beyond the aims and scope of the present context, we will refrain from considering the six coolest stars for further analysis in this article.

Adopting the spectroscopic parameters for the remaining warmer stars, we derive the abundances of a range of elements from Na to Ce. We adopt the new solar values of Asplund et al. (2009) to obtain elemental abundances relative to the Sun. The final stellar abundances in the [X/H] form are presented in Table 4. The results are displayed graphically in Figs 3–11, where we overplot the abundances of the disc field stars from Bensby et al. (2005) (grey crosses) where available.

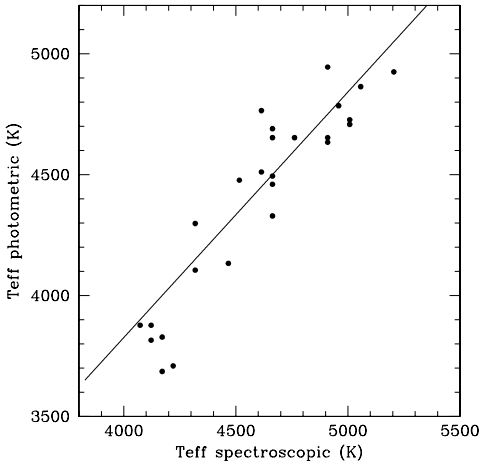

Figure 1. Effective temperatures via the $B-V$ colour calibrations of Alonso et al; 1999 versus the spectroscopic temperatures. The solid line is the average difference, where the spectroscopic values are hotter on average by ∼150 K.

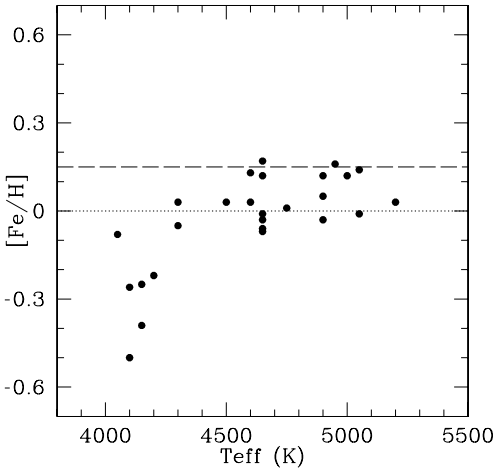

Figure 2. [Fe/H] versus effective temperature. The dotted line represents the solar level and the dashed line represents the Hyades open cluster metallicity.

4.2.1 Errors in the derived abundances

The possible sources of uncertainty are the errors associated with EW measurements, continuum placement and stellar parameters, as well as the number of lines used to calculate the final abundances. The typical error in the stellar parameters were estimated to be $\delta T_{\rm eff} = 50$ K, $\delta \log g = 0.1$ cm s^{-2} and $\delta\xi = 0.1$ km s^{-1} based on our spectroscopic derivation. The error in EWs was estimated by repeated measurements of each line during the EW measurement process. The measurement error for the synthesized elements is the uncertainty on the best-fitting abundance value. Abundance dependencies on the stellar parameters and the measurement error for each element are given in Table 5 for the star HD 78402, which has a mid-range $T_{\rm eff}$ and log g.

S, Zn and Zr have uncertainties larger than 0.1 dex. For S and Zn, the dominant error is the large variation between the two lines studied per element, while Zr is most sensitive to temperature. No trends with $T_{\rm eff}$ were seen for any of the elements, but it is possible that the weak lines are affected by blending, giving rise to inaccurate abundances. Na, Sc and Co have uncertainties larger than 0.05 dex, while all other element uncertainties are within the

Table 4. Elemental abundances.

ID	[Fe/H]	[Na/H]	[Mg/H]	[Al/H]	[Si/H]	[S/H]	[Ca/H]	[Sc/H]	[Ti/H]	[Cr/H]	[Mn/H]	[Co/H]	[Ni/H]	[Zn/H]	[Zr/H]	[Ba/H]	[La/H]	[Ce/H]
HD 84598	−0.01	0.17	0.10	0.05	0.05	−0.06	0.02	0.04	−0.08	−0.02	−0.08	-0.12	−0.05	0.07	0.16	0.42	0.10	0.13
HD 83234	0.03	0.11	0.00	0.31	0.15	0.21	0.01	0.05	0.20	0.08	0.03	0.06	0.07	−0.04	0.49	0.00	0.26	0.37
HD 81278	0.12	0.08	0.13	0.20	0.27	0.38	0.14	0.15	0.08	0.12	0.12	0.28	0.21	0.38	0.06	0.40	0.16	0.20
HD 80571	0.05	0.02	0.03	0.12	0.17	0.02	−0.05	0.14	−0.11	−0.04	−0.08	0.03	0.04	0.10	0.04	0.17	0.02	0.10
HD 78402	−0.03	−0.02	0.15	0.14	0.05	0.01	0.07	0.17	0.19	0.07	−0.03	0.03	0.07	0.15	0.36	0.47	0.36	0.45
HD 78204	0.14	0.34	0.22	0.24	0.18	0.17	0.19	−0.02	0.04	0.16	0.16	0.09	0.12	0.02	0.34	0.37	0.18	0.22
HD 78002	0.12	0.32	0.19	0.18	0.23	0.33	0.16	0.14	0.07	0.14	0.13	0.12	0.16	0.16	0.19	0.40	0.15	0.22
HD 77241	0.13	0.34	0.19	0.36	0.41	0.38	0.08	0.14	0.09	0.16	0.16	0.31	0.24	0.24	0.14	0.03	0.00	0.04
HD 76128	0.17	0.11	0.10	0.25	0.32	0.29	0.03	0.28	0.05	0.15	0.12	0.20	0.19	0.55	0.16	0.37	0.16	0.25
HD 75058	−0.03	0.02	0.04	0.07	0.12	0.02	0.02	0.00	−0.09	−0.06	−0.05	0.05	−0.01	0.25	−0.15	0.15	−0.07	−0.05
HD 74900	−0.01	0.07	0.14	0.20	0.23	0.15	0.01	0.11	0.00	−0.02	−0.07	0.10	0.05	0.32	−0.05	0.10	−0.02	0.05
HD 74529	0.12	0.19	0.04	0.21	0.22	0.27	0.03	0.05	−0.10	0.02	−0.04	0.04	0.01	0.16	0.08	0.09	−0.05	−0.05
HD 74166	−0.05	0.19	0.08	0.21	0.02	0.24	−0.13	−0.11	−0.17	−0.09	–	-0.13	−0.11	−0.18	0.11	–	–	–
HD 74165	0.03	0.11	0.12	0.28	0.15	0.15	−0.01	0.01	−0.01	0.05	−0.03	0.05	0.00	0.14	0.14	0.02	−0.06	0.03
HD 73829	−0.07	0.07	−0.02	0.07	0.15	0.00	−0.11	−0.08	−0.12	−0.11	0.01	-0.04	−0.06	0.04	−0.03	0.00	0.00	0.05
HD 73657	0.03	0.18	0.07	0.17	0.25	0.15	−0.09	−0.08	−0.15	−0.06	−0.04	-0.04	−0.03	0.02	0.03	−0.07	−0.02	0.02
HD 72630	0.16	0.28	0.25	0.28	0.24	0.19	0.19	0.16	0.11	0.19	0.17	0.18	0.17	0.25	0.31	0.43	0.18	0.20
HD 72320	0.03	0.16	0.07	0.12	0.09	0.05	0.08	0.04	0.00	0.05	0.01	-0.09	−0.02	0.05	0.20	0.57	0.30	0.40
HD 69836	0.01	−0.01	0.09	0.12	0.17	0.06	−0.03	0.11	−0.09	−0.04	−0.01	0.07	0.07	0.19	−0.02	0.30	0.05	0.15
HD 122721	−0.06	0.00	0.01	0.08	0.11	0.00	−0.04	0.02	−0.12	−0.07	−0.04	-0.03	−0.02	0.12	−0.01	0.37	0.15	0.22

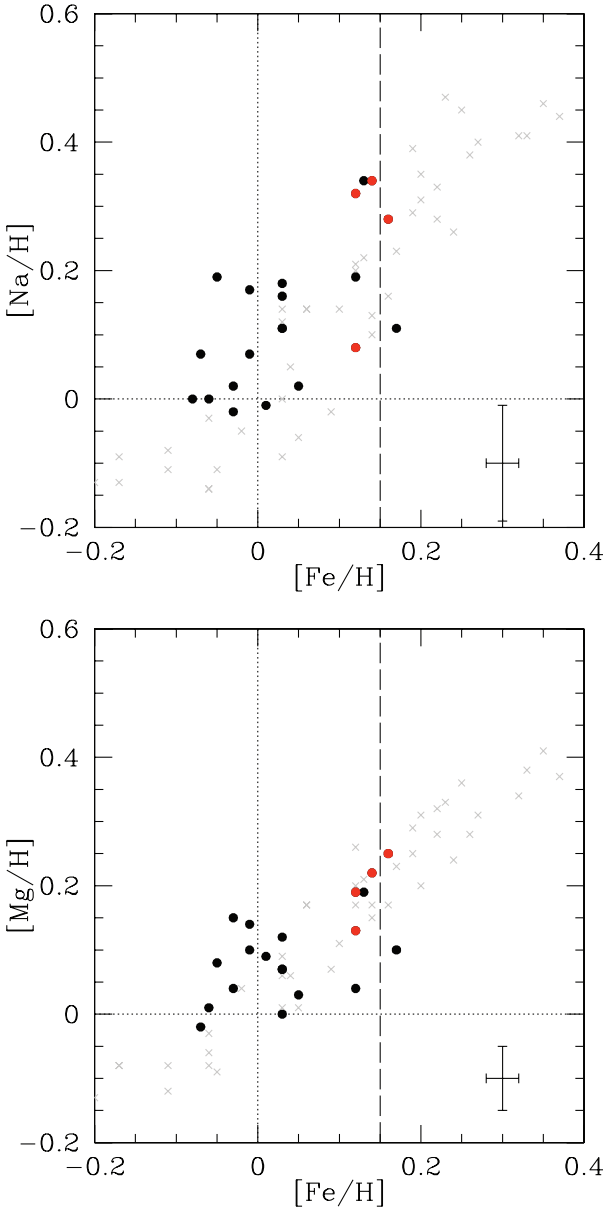

Figure 3. [X/H] versus [Fe/H] for the sample stars (filled circles). The grey crosses are thin disc stars of Bensby et al. (2005).

0.05 dex level. Na abundance accuracy varies with both the error in EW measurement and the line-to-line scatter. For Sc and Co, the total uncertainty is from a combination of factors given in Table 5. Note that our analysis of Sc and Co did not take into account possible effects of hyperfine structure, as we assumed such effects were negligible for our targeted lines (McWilliam et al. 1995). Likewise no NLTE effects were considered in this study. Such effects however may result in a larger scatter and overestimated abundances.

5 ORIGIN OF THE HYADES SUPERCLUSTER

5.1 Chemical tagging

In the case of a dispersing stellar aggregate, where the member stars were all formed from a common protocluster gas cloud, we expect to find chemical homogeneity (De Silva et al. 2006, 2007b).

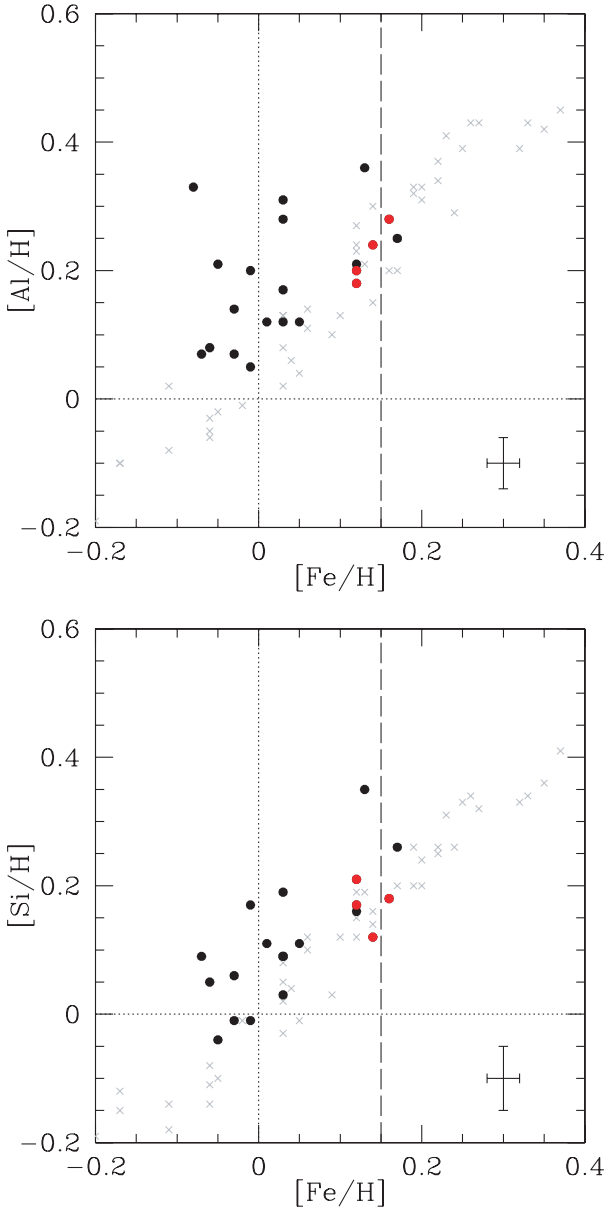

Figure 4. [X/H] versus [Fe/H] for the sample stars (filled circles). The grey crosses are thin disc stars of Bensby et al. (2005).

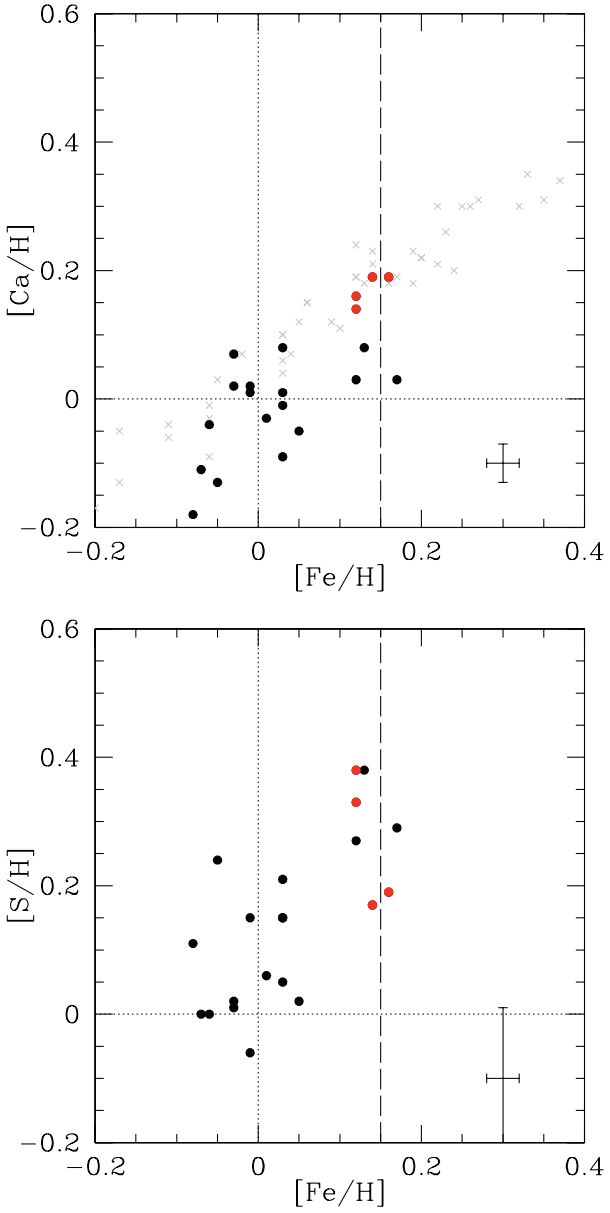

Figure 5. [X/H] versus [Fe/H] for the sample stars (filled circles). The grey crosses are thin disc stars of Bensby et al. (2005).

The abundance results presented in Section 4.2 show the abundance distribution clustered around [Fe/H] = 0.0 and [Fe/H] = 0.15. From Fig. 2 we see that the majority of the stars are located around solar metallicity, while seven stars have high metallicities comparable to the Hyades open cluster metallicity. Note that the [Fe/H] distribution is such that there is a clear gap between $0.05 < [Fe/H] < 0.1$, rather than a heterogeneous spread across the sample. The individual element abundance plots show that four of these seven metal-rich stars (HD 81278, HD 78204, HD 78002, HD 72630) are clumped together across many of the elements. The standard deviation in abundance for these four stars is less than 0.05 for all elements except for Na, S, Sc, Co, Zn and Zr. Note that these elements also have a higher abundance uncertainty, whereas all other elements were measured to 0.05 dex internal accuracy.

We compare our sample star abundances against the thin disc abundances of Bensby et al. (2005). The majority of our sample contains solar-level metallicity stars, which match the field star abundances well, implying that our sample of potential Hyades supercluster is dominated by field stars, rather than those from a dispersing stellar aggregate. This supports the case of the kinematically defined Hyades supercluster being a transient feature caused by disc dynamics. Regarding those stars at [Fe/H] $\sim$ 0.15, the disc field also contains similar high-metallicity stars which overlap with the Hyades open cluster abundances. We ask, how likely is it that the higher metallicity stars in our sample are Hyades-related, and not just metal-rich field stars?

First, Na is enhanced relative to the field stars. This is seen for some solar-metallicity-level stars as well as few of the metal-rich stars. A possible explanation for this is the abundance variations between giants and dwarfs (De Silva et al. 2009). It is possible that the internal mixing mechanism have enhanced the natal Na abundances in some of these giant stars, hence making the measured abundances less reliable for chemical tagging. More interestingly, Ba is much enhanced among the four metal-rich stars relative to the field star

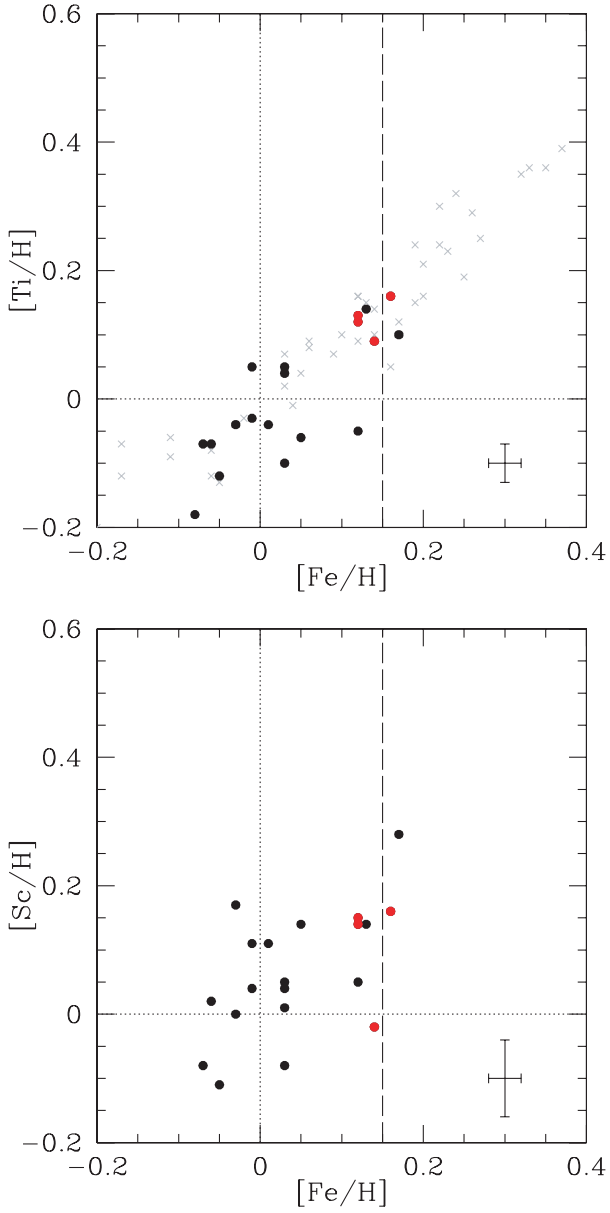

Figure 6. [X/H] versus [Fe/H] for the sample stars (filled circles). The grey crosses are thin disc stars of Bensby et al. (2005).

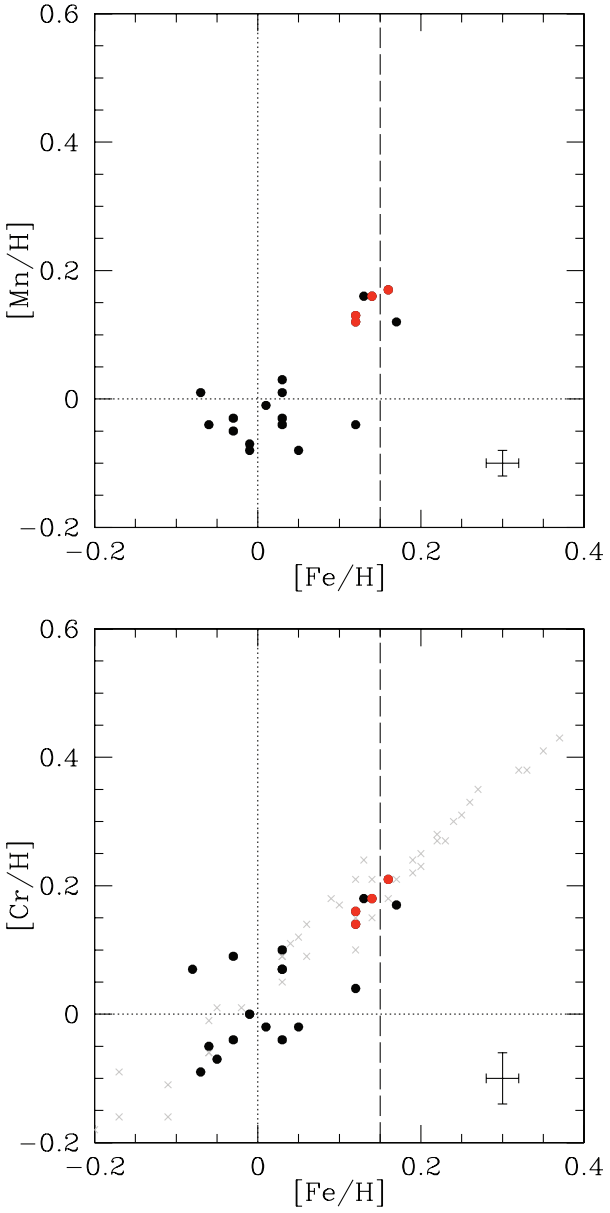

Figure 7. [X/H] versus [Fe/H] for the sample stars (filled circles). The grey crosses are thin disc stars of Bensby et al. (2005).

abundances. A similar Ba enhancement is seen in the Hyades open cluster based on high-resolution abundance analysis (De Silva et al. 2006). In fact the observed enhancement in these four stars for La and Ce is also seen in the Hyades open cluster. Using the results of De Silva et al. (2006), the Hyades open cluster mean abundances are [Ba/H] = 0.45, [La/H] = 0.10 and [Ce/H] = 0.17, when scaled to the solar values of Asplund et al. (2009) which we employ in this analysis. The average abundance values of the four metal-rich stars in this study are [Ba/H] = 0.40, [La/H] = 0.16 and [Ce/H] = 0.2. This is in remarkable agreement with the Hyades open cluster abundances taking into account the measurement uncertainties in the two studies. We also attempted to compare our results with those by Paulson et al. (2003) for the Hyades open cluster for α-element and Fe-peak element abundances. However, in our investigation we were unable to determine their absolute solar-abundance scale to make a useful comparison possible. Since their work was focused on differential abundances relative to their measured solar spectrum, many unquantifiable systematics likely exist between the two studies.

The combination of Hyades open cluster-like abundance patterns for Fe and heavy elements and the high level of abundance homogeneity seen among the four metal-rich stars of our sample, suggest that these four stars were once part of the Hyades star-forming aggregates, but are now dispersed elsewhere. Combining this scenario with the observed spread in abundances for the majority of our sample stars adds further mystery to the origin of the Hyades supercluster. Therefore we now turn to exploring the kinematical membership criteria.

While open cluster members are easily determined from radial velocities, memberships for dispersed groups are based on the star's *UVW* space motion. However, the exact criteria for selecting members remain somewhat uncertain. Eggen's method of isolating dispersed members required member stars to have the same *V* velocity, i.e. in the direction of the Galactic rotation, based on epicycle

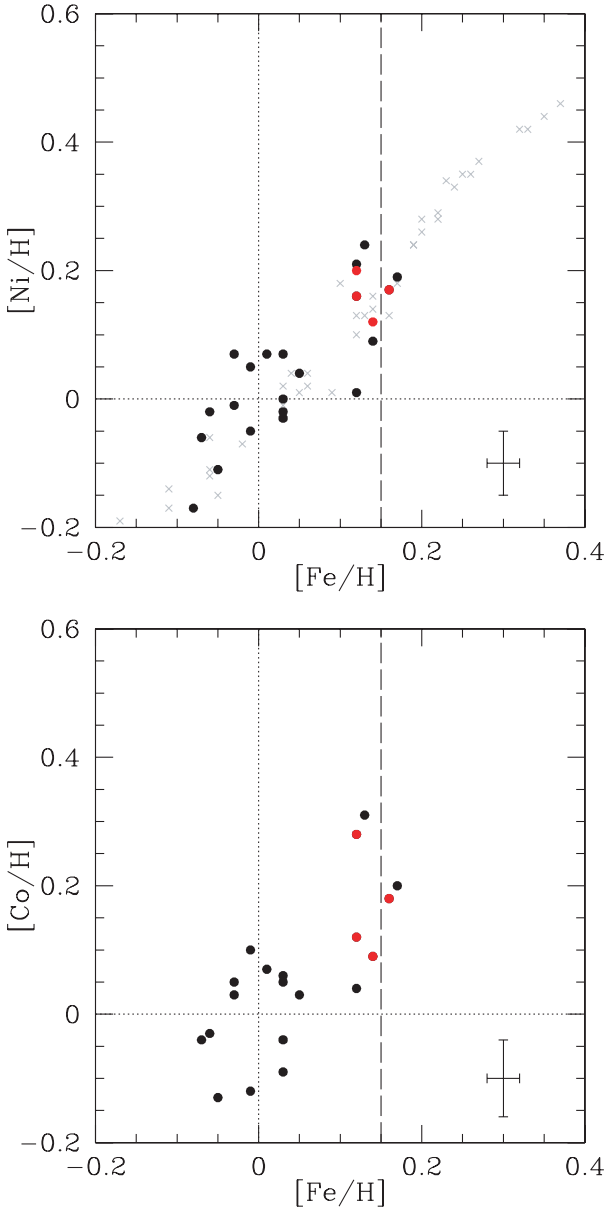

Figure 8. [X/H] versus [Fe/H] for the sample stars (filled circles). The grey crosses are thin disc stars of Bensby et al. (2005).

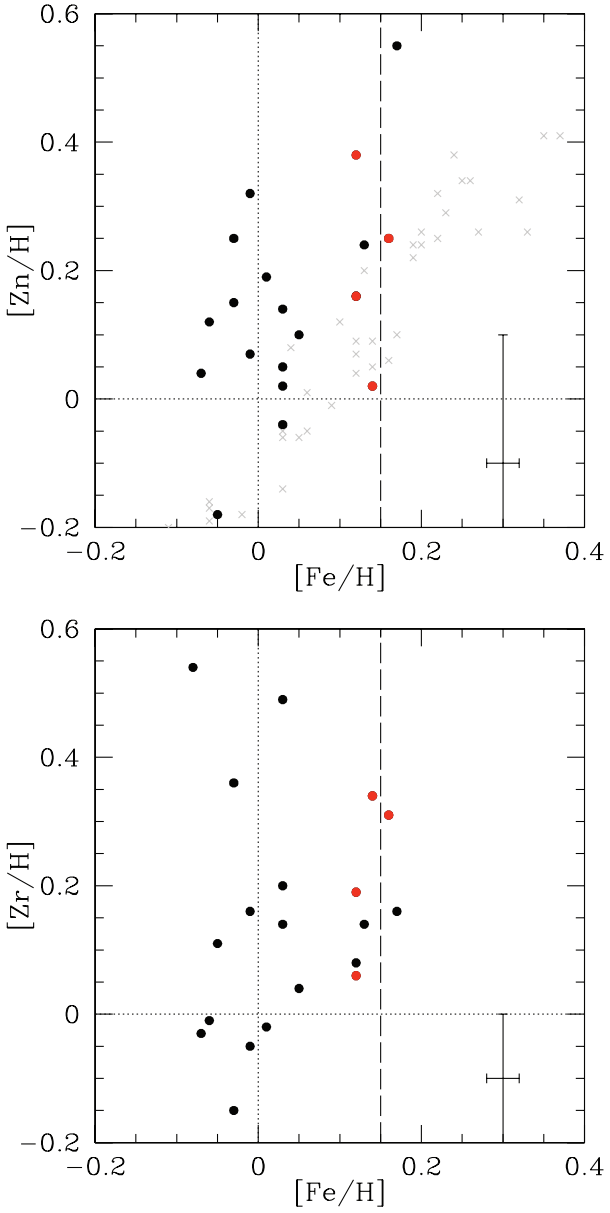

Figure 9. [X/H] versus [Fe/H] for the sample stars (filled circles). The grey crosses are thin disc stars of Bensby et al. (2005).

theory. However, recent more realistic Galaxy dynamical models show that such a clump in V is not necessary for membership to a moving group or supercluster; rather a small *tilt* or *curve* in the distribution in the U–V plane is the dynamical signature of a dispersed aggregate (Skuljan, Cottrell & Hearnshaw 1997; Feltzing & Holmberg 2000; Helmi et al. 2006; De Silva et al. 2007a). Along with our abundance results, we explore the membership probabilities of our sample stars using the positions on the colour–magnitude diagram and the stellar kinematics.

5.2 Distances and colour–magnitude diagram

A fundamental property of a star cluster, as a single-generation population, is that it displays a clear evolutionary sequence of stars of various masses in the colour–magnitude diagram (CMD), contrary to the field star population which contains a large range in age and metallicity. We compare our sample stars against the Hyades open cluster CMD. Since only 10 stars in our sample have accurate distance measurements in the literature, we plot the spectroscopically derived Teff versus log g of the studied sample. Fig. 12 shows our sample together with the spectroscopically derived stellar parameters of the Hyades open cluster dwarfs (open circles) obtained by Primas et al. (in preparation). We can confidently make this comparison because the $T_{\rm eff}$ and log g for both open cluster dwarfs and the supercluster giants were derived via the same methodology for similar quality UVES spectra, using the same Fe I and Fe II lines and model atmospheres. To guide the eye, overlaid in Fig. 12 is an isochrone of 0.7 Gyr, $Z = 0.025$ from Girardi et al. (2000), which closely corresponds to the Hyades open cluster age and metallicity. The larger red circles are the four Hyades open cluster-like stars discussed above in Section 5.1.

Fig. 12 shows that all of our sample stars are consistent with a Hyades-aged isochrone. However, our chemical abundance results

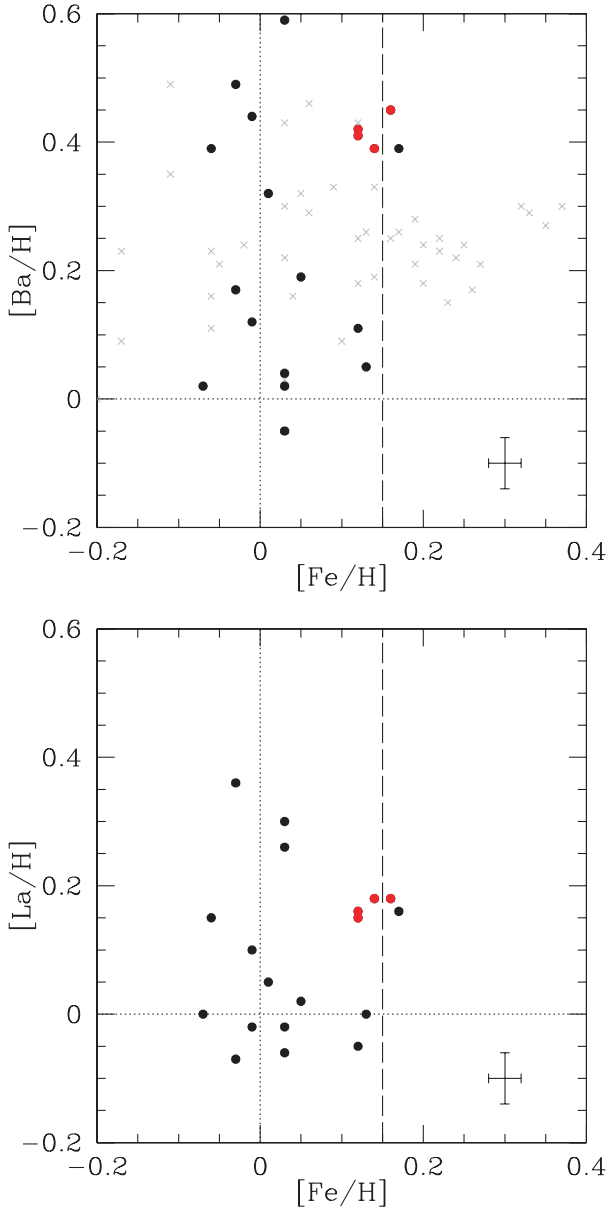

Figure 10. [X/H] versus [Fe/H] for the sample stars (filled circles). The grey crosses are thin disc stars of Bensby et al. (2005).

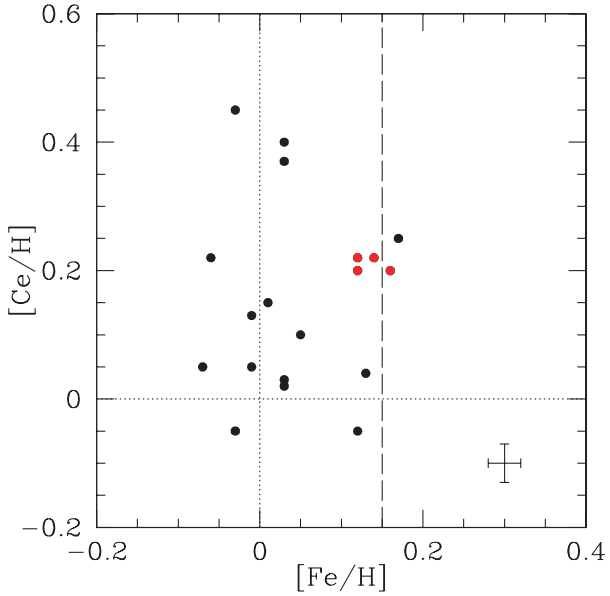

Figure 11. [X/H] versus [Fe/H] for the sample stars (filled circles). The grey crosses are thin disc stars of Bensby et al. (2005).

in Section 5.1 show that only four stars are likely associated with the Hyades star-forming event. Therefore lying along the isochrone alone is not a sufficient condition for group membership.

Using Fig. 12, we can use the best-fitting isochrone to derive the distances for each of our sample stars. By comparing the location of each star on the isochrone, we determined the equivalent absolute V magnitude from the isochrone. With the determined absolute magnitudes and the known apparent magnitudes, we derive the distances of the sample stars. Table 6 lists the derived distances and Fig. 13 shows the location of our stars in X-Y and X-Z spatial coordinates, where X-Y is in the Galactic plane. The open circle represents the location of the Hyades open cluster. The four red stars with Hyades-like abundances lie outside the open cluster and are not present members of the bound open cluster.

5.3 Radial velocities

Radial velocities for our target stars were calculated from our high-resolution spectra using the DAOSPEC code (Stetson & Pancino 2008), which matches lines with measured equivalent widths against a line list. A comprehensive and realistic line list for stellar spectra was obtained using the *extract stellar* on the VALD data base. We used our line list for a [Fe/H] $= -0.7$, $T_{\rm eff} = 5500$, $\log g = 4.25$, $\xi = 1.3$ star, where for our radial velocity calculation of Hyades stars we can expect little effect of the stellar parameter differences. DAOSPEC was run on three 100-Å intervals at 5600–5700, 5800–5900 and 6000–6100 Å where DAOSPEC returns a radial velocity estimate with a corresponding dispersion by comparison with the line list. The radial velocity was obtained for each star from a weighted average of the three measurements, after correcting to heliocentric radial velocity. The final values are listed in column 2 of Table 7.

5.4 U, V, W velocities

Using the derived distances, radial velocities and proper motions from the Tycho-2 catalogue, we calculate the space velocities assuming a right-handed Cartesian UVW velocities centred on the solar position, with the U velocity positive towards the Galactic centre. Velocities were corrected to the local standard of rest (LSR) using the peculiar motion of the Sun given by Dehnen (1998) of 10, 5.3, 7.2 km s^{-1} in U, V and W, respectively. Errors in UVW were calculated using a Monte Carlo simulation of 1000 realizations to propagate the errors in distance (where we assumed a 20 per cent error), proper motion and radial velocity into the space velocities, from whence the dispersions were calculated. The results are tabulated in Table 7 and the V versus U values are plotted in Fig. 14, where the dotted line marks the V velocity of the Hyades open cluster and the red circles highlight the four Hyades open cluster-like stars discussed earlier in Section 5.1.

We find that our sample stars are located within ± 20 km s^{-1} of the Hyades cluster V velocity. Stars with large velocity deviations are most likely unrelated field stars based on the kinematical membership criterion. This shows that the hypothesis used by Wilson

Table 5. Abundance sensitivities for the star HD 78402.

Parameter	Fe	Na	Mg	Al	Si	S	Ca	Sc	Ti	Cr	Mn	Co	Ni	Zn	Zr	Ba	La	Ce
$T_{\rm eff} \pm 50$	±0.01	±0.04	±0.03	∓0.02	±0.03	±0.01	±0.02	∓0.01	±0.01	±0.02	±0.01	±0.01	±0.01	±0.05	±0.08	±0.02	±0.02	±0.02
$\log g \pm 0.1$	±0.01	∓0.02	∓0.04	±0.01	∓0.04	∓0.01	∓0.01	±0.01	±0.04	±0.02	0.0	±0.02	±0.03	±0.01	±0.02	±0.01	±0.03	0.00
$\xi \pm 0.1$	∓0.02	∓0.02	∓0.02	∓0.01	∓0.04	±0.02	∓0.04	∓0.03	∓0.05	±0.01	∓0.01	±0.02	0.00	±0.01	±0.02	∓0.03	∓0.02	0.00
Δ EW/Synth	±0.02	±0.06	±0.05	±0.04	±0.03	±0.03	±0.03	±0.03	±0.02	±0.02	±0.02	±0.02	±0.02	±0.03	±0.03	±0.02	±0.02	±0.02
σ(line-to-line)	±0.01	±0.07	±0.03	–	±0.02	±0.1	±0.02	±0.06	±0.03	±0.01	±0.01	±0.05	±0.02	±0.2	±0.03	±0.04	–	–
Total	±0.02	±0.09	±0.05	±0.04	±0.05	±0.11	±0.03	±0.06	±0.03	±0.04	±0.02	±0.06	±0.05	±0.2	±0.1	±0.04	±0.04	±0.03

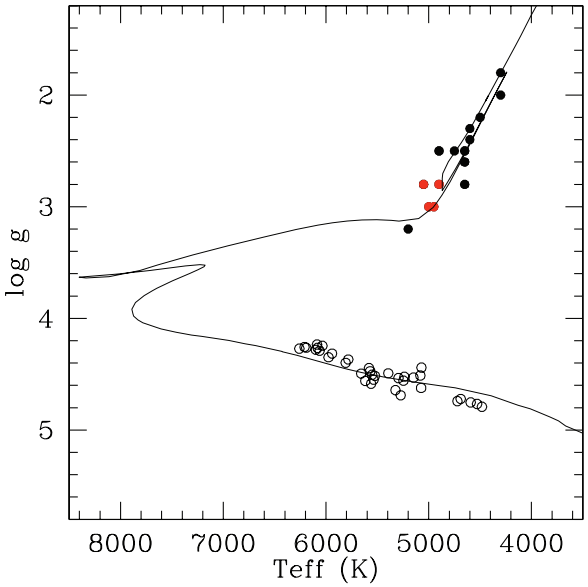

Figure 12. Spectroscopic $T_{\rm eff}$ versus $\log g$ of the supercluster sample and the Hyades open cluster dwarfs (open circles). The red circles are the four metal-rich stars discussed in Section 5.1.

Table 6. Absolute magnitudes and distances.

Star ID	M (V)	Distance (pc)
HD 84598	1.355	164.8
HD 83234	1.162	300.3
HD 81278	1.250	278
HD 80571	0.612	284.2
HD 78402	0.612	713.8
HD 78204	1.345	523.6
HD 78002	1.345	415.9
HD 77241	−0.052	1015
HD 76128	−0.369	498.7
HD 75058	0.686	447.5
HD 74900	0.620	293.8
HD 74529	0.620	361.4
HD 74166	−0.725	464.5
HD 74165	0.417	547.8
HD 73829	0.555	590.2
HD 73657	−0.252	415.3
HD 72630	1.313	429.9
HD 72320	1.285	341.2
HD 69836	0.246	460
HD 122721	0.555	523.6

to select probable Hyades supercluster members was not efficient. The four metal-rich stars with Hyades open cluster-like abundances lie tightly clustered within 3 km s^{-1} of the Hyades cluster velocity, along with several other stars which did not have similar elemental abundances. To estimate the expected number of background stars with Hyades-like motion and metallicity, we queried the Besancon stellar population model (Robin et al. 2003) based on our sample selection criteria. The model was queried for stars within 600 pc, with magnitude $V < 10$, between galactic longitudes $253 < l < 279$ and latitudes $-3 < b < 3$. The [Fe/H] versus V velocity of the model stars, as well as our sample stars are plotted in Fig. 15. The red circles are the four stars with Hyades open cluster-like abundances. Two of those stars have almost identical [Fe/H] values and V velocities, hence they are overlapping in Fig. 15. Another star,

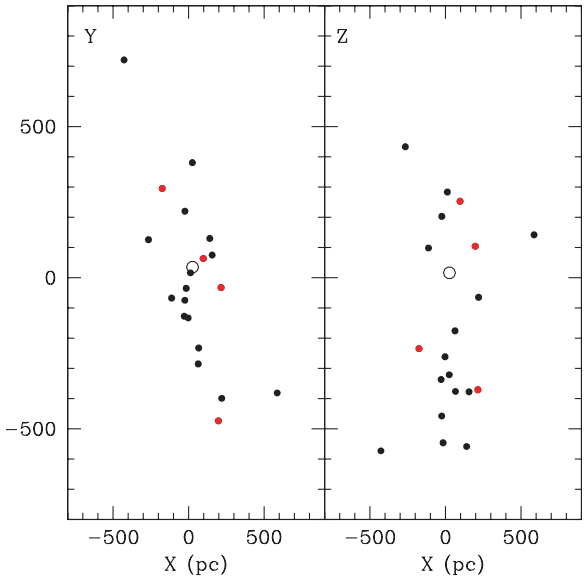

Figure 13. The location of the sample stars in *X*-*Y* and *X*-*Z* plane, where *X*-*Y* is in the Galactic plane. The open circle represents the Hyades open cluster and the red stars are the four metal-rich stars with Hyades-like abundances discussed in Section 5.1.

HD 77241, also lies close to the open cluster velocity. Despite having a similarly high metallicity, this star did not have similar abundance levels across the other studied elements. Enforcing both the kinematical and chemical tagging criteria, we confirm that these four stars are likely to be former members of the Hyades open cluster.

6 CONCLUSION

We have obtained high-resolution spectra of 45 proposed Hyades supercluster members, which were selected based on early estimates of the targets' metallicity and position along the expected dispersion orbit of the Hyades supercluster, as well as F-type *Hipparcos* stars from Eggen (1998). The observing results showed that only 26 stars were suitable for a detailed abundance analysis. The abundance distribution showed a double-peaked distribution, with two clear clustering of stars – one around solar metallicity and the other around Hyades open cluster metallicity.

Four of the stars with Hyades open cluster metallicity also shared similar abundance patterns, with the star-to-star scatter being within 0.05 across all elements except for Na, S, Sc, Co, Zn and Zr. Possible deviations due to stellar evolutionary effects as well as larger abundance uncertainty in this analysis make these six elements less reliable for chemical tagging than the other elements analysed in this study. Further, the four stars' abundances for Ba, La and Ce match the abundances observed in the Hyades open cluster. These heavy elements are produced predominantly via the slow neutron capture process, where the likely sites of formation are Type II supernova explosion. Therefore, the heavy element abundances are not modified during the lifetime of the giant and subgiant stars we have studied, and the measured abundances should represent the abundance levels laid out during the stars' birth in a protocluster cloud.

Examining the space velocities of our targets revealed that our sample stars are within $\pm 20\,\mathrm{km\,s^{-1}}$ of the Hyades open cluster *V* velocity. Those velocity outliers are most likely to be non-members of the kinematically defined Hyades supercluster. Applying both kinematical and chemical criteria, we find that four stars are likely dispersed members from an earlier Hyades star-forming event. These four stars share Hyades-like kinematics and chemical abundances, but spatially they are located away from the Hyades open cluster. Therefore, these four stars are clearly supercluster members rather than open cluster members. The rest of the stars are either non-members of the supercluster or they are kinematically members of a comoving group, but are otherwise unrelated to the Hyades star-forming event.

The presented results are primarily a test of the Hyades cluster disruption hypothesis of Wilson (1990). We find ∼15 per cent of his sample are supercluster members based on kinematics and chemical abundances. Our study only included one slow rotating star from Eggen (1998), hence we are unable to test the validity of

Table 7. Radial and Galactic space velocities.

Star ID	RV ($\mathrm{km\,s^{-1}}$)	RV error	*U* ($\mathrm{km\,s^{-1}}$)	*U* error	*V* ($\mathrm{km\,s^{-1}}$)	*V* error	*W* ($\mathrm{km\,s^{-1}}$)	*W* error
HD 84598	1.07	0.71	15.05	0.51	4.41	0.72	1.81	0.59
HD 83234	11.42	0.51	−8.68	13.42	−8.78	1.77	16.02	9.15
HD 81278	20.18	0.54	−26.87	10.28	−17.93	0.72	26.15	10.06
HD 80571	15.13	0.48	−77.95	35.93	−8.63	1.14	25.25	35.33
HD 78402	18.12	0.54	59.80	35.68	−13.41	1.02	32.01	39.13
HD 78204	19.51	0.68	−37.43	20.28	−15.27	0.89	10.43	21.79
HD 78002	25.39	0.61	−22.19	15.41	−17.71	0.83	5.41	17.17
HD 77241	18.74	0.58	−64.74	29.73	−12.43	1.73	17.54	33.33
HD 76128	40.41	0.57	3.98	11.96	−33.82	1.28	32.03	18.06
HD 75058	27.90	0.49	10.71	29.27	−26.65	3.56	−54.89	36.91
HD 74900	21.12	0.48	−18.49	20.31	−12.29	2.58	−13.73	25.69
HD 74529	11.50	0.55	16.59	19.29	−4.19	2.71	−39.80	24.88
HD 74166	18.15	0.66	−4.18	5.47	−11.01	1.06	6.11	6.61
HD 74165	24.77	0.59	−74.18	43.84	−6.30	6.59	−26.33	57.07
HD 73829	17.43	0.53	39.52	14.36	−16.36	2.34	11.66	18.65
HD 73657	28.84	0.59	−19.58	6.99	−19.51	1.25	11.73	9.31
HD 72630	25.62	0.60	−24.37	17.40	−14.92	3.08	13.99	11.47
HD 72320	27.73	0.61	−1.57	3.95	−20.85	0.99	3.87	5.54
HD 69836	38.72	0.64	−62.88	17.95	−13.40	5.28	10.21	27.25
HD 122721	−28.80	0.47	−43.79	36.83	−21.92	32.68	−9.04	14.38

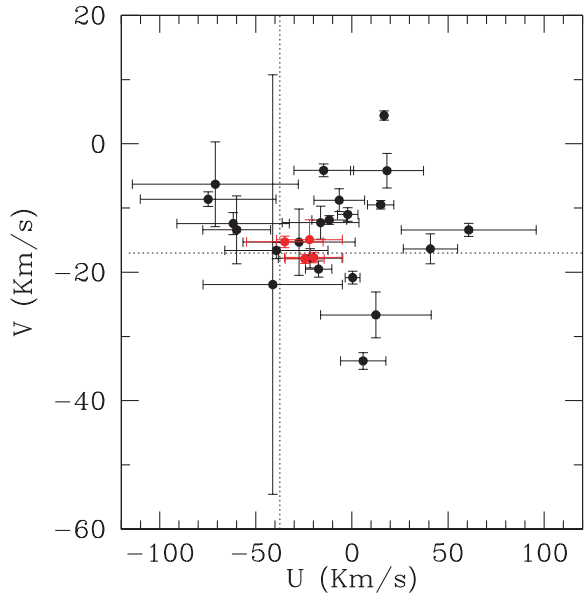

Figure 14. Galactic *V* velocity versus *U* velocity for the sample stars. Red stars are the four metal-rich stars discussed in Section 5.1. The dotted lines mark the Hyades open cluster velocities.

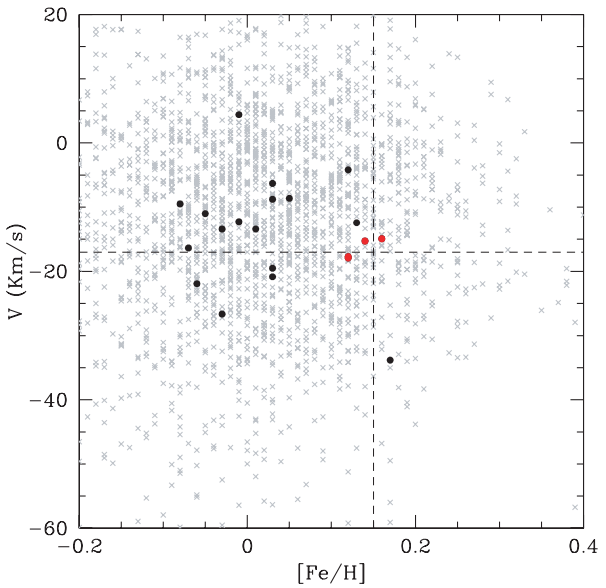

Figure 15. Galactic *V* velocity versus [Fe/H] for the sample stars. Red stars are the four metal-rich stars discussed in Section 5.1. The grey crosses are the output from the Besancon stellar population model for stars based on our selection criteria.

his sample. From our results, we conclude that the kinematically defined Hyades supercluster is made up at least partly of dispersed Hyades cluster stars. Recently we became aware of a similar study by Pompeia et al. (2011) who also carried out a spectroscopic analysis of other members of the Hyades supercluster, and their results are consistent with our findings. Further studies of the Hyades supercluster, especially targeting kinematically defined dwarf stellar members, are encouraged.

ACKNOWLEDGMENTS

GMDS would like to thank F. Primas for the use of the stellar parameters for the Hyades open cluster dwarfs based on a new Hyades open cluster abundance analysis in preparation.

REFERENCES

Allende Prieto C., Barklem P. S., Lambert D. L., Cunha K., 2004, A&A, 420, 183
Alonso A., Arribas S., Martinez-Roger C., 1996, A&A, 140, 261
Antoja T., Figueras F., Fernández D., Torra J., 2008, A&A, 490, 135
Asplund M., Grevesse N., Sauval A., Scott P., 2009, ARA&A, 47, 481
Bensby T., Feltzing S., Lundström I., 2003, A&A, 410, 527
Bensby T., Feltzing S., Lundström I., Ilyin I., 2005, A&A, 433, 185
Bensby T., Oey M. S., Feltzing S., Gustafsson B., 2007, ApJ, 655, 89
Blackwell D. E., Ibbetson P. A., Petford A. D., Shallis M. J., 1979a, MNRAS, 186, 633
Blackwell D. E., Petford A. D., Shallis M. J., 1979b, MNRAS, 186, 657
Blackwell D. E., Lynas-Gray A. E., Smith G., 1995, A&A, 296, 217
Bovy J., Hogg D. W., 2010, ApJ, 717, 617
Bovy J., Hogg D. W., Roweis S. T., 2009, ApJ, 700, 1794
Bubar E. J., King J. R., 2010, AJ, 140, 293
Castelli F., Gratton R. G., Kurucz R. L., 1997, A&A, 318, 841
De Silva G. M., Sneden C., Paulson D. B., Asplund M., Bland-Hawthorn J., Bessell M. S., Freeman K. C., 2006, AJ, 131, 455
De Silva G. M., Freeman K. C., Bland-Hawthorn J., Asplund M., Bessell M. S., 2007a, AJ, 133, 694
De Silva G. M., Freeman K. C., Asplund M., Bland-Hawthorn J., Bessell M., Collet R., 2007b, AJ, 133, 1161
De Silva G. M., Gibson B. K., Lattanzio J., Asplund M., 2009, A&A, 500, L25
Dehnen W., 1998, AJ, 115, 2384
Eggen O. J., 1958, MNRAS, 118, 154
Eggen O. J., 1959a, Observatory, 79, 88
Eggen O. J., 1959b, Observatory, 79, 182
Eggen O. J., 1965, Observatory, 85, 191
Eggen O. J., 1969, PASP, 81, 553
Eggen O. J., 1970, PASP, 82, 99
Eggen O. J., 1971, PASP, 83, 271
Eggen O. J., 1974, PASP, 86, 162
Eggen O. J., 1977, ApJ, 215, 812
Eggen O. J., 1978a, ApJ, 222, 191
Eggen O. J., 1978b, ApJ, 222, 203
Eggen O. J., 1983, AJ, 88, 813
Eggen O. J., 1992a, AJ, 104, 1906
Eggen O. J., 1992b, AJ, 104, 1482
Eggen O. J., 1996, AJ, 111, 1615
Eggen O. J., 1998, AJ, 115, 2453
Famaey B., Jorissen A., Luri X., Mayor M., Udry S., Dejonghe H., Turon C., 2005, A&A, 430, 165
Feltzing S., Holmberg J., 2000, A&A, 357, 153
Freeman K., Bland-Hawthorn J., 2002, ARA&A, 40, 487
Girardi L., Bressan A., Bertelli G., Chiosi C., 2000, A&AS, 141, 371
Gratton R. G., Bonanno G., Claudi R. U., Cosentino R., Desidera S., Lucatello S., Scuderi S., 2001, A&A, 377, 123
Helmi A., Navarro J. F., Nordström B., Holmberg J., Abadi M. G., Steinmetz M., 2006, MNRAS, 365, 1309
Houk N., 1982, Michigan Cat. Two-dimensional Spectral Types HD Star, 3, 12
Kupka F., Piskunov N. E., Ryabchikova T. A., Stempels H. C., Weiss W. W., 1999, A&AS, 138, 119
Kupka F., Ryabchikova T. A., Piskunov N. E., Stempels H. C., Weiss W. W., 2000, Baltic Astron., 9, 590
McWilliam A., Preston G. W., Sneden C., Searle L., 1995, AJ, 109, 2757

Minchev I., Boily C., Siebert A., Bienayme O., 2010, MNRAS, 407, 2122
Pancino E., Carrera R., Rossetti E., Gallart C., 2010, A&A, 511, 56
Paulson D. B., Sneden C., Cochran W. D., 2003, AJ, 125, 3185
Piskunov N. E., Kupka F., Ryabchikova T. A., Weiss W. W., Jeffery C. S., 1995, A&AS, 112, 525
Pompeia L. et al., 2011, MNRAS, in press
Prochaska J. X., McWilliam A., 2000, ApJ, 537, L57
Prochaska J. X., Naumov S. O., Carney B. W., McWilliam A., Wolfe A. M., 2000, AJ, 120, 2513
Robin A. C., Reyl C., Derrire S., Picaud S., 2003, A&A, 409, 523
Ryabchikova T. A., Piskunov N. E., Stempels H. C., Kupka F., Weiss W. W., 1997, Baltic Astron., 6, 244
Skuljan J., Cottrell P. L., Hearnshaw J. B., 1997, in ESA SP-402: Hipparcos - Venice '97, 525
Sneden C. A., 1973, PhD thesis, Univ. Texas
Stetson P., Pancino E., 2008, PASP, 120, 1332
Wilson G., 1990, PhD thesis, Australian Natl Univ.
Yong D., Lambert D. L., Allende Prieto C., Paulson D. B., 2004, ApJ, 603, 697
Zhao J., Zhao G., Chen Y., 2009, ApJ, 692, L113

SUPPORTING INFORMATION

Additional Supporting Information may be found in the online version of this article:

Table 2. Line list.

Please note: Wiley-Blackwell are not responsible for the content or functionality of any supporting materials supplied by the authors. Any queries (other than missing material) should be directed to the corresponding author for the article.

This paper has been typeset from a TEX/LATEX file prepared by the author.